# High-pressure tuning of *d–d* crystal-field electronic transitions and electronic band gap in $Co(IO_3)_2$

A. Liang,[1] F. Rodríguez,[2] P. Rodríguez-Hernandez,[3] A. Muñoz,[3] R. Turnbull,[1] and D. Errandonea[1]

[1]*Departamento de Física Aplicada—ICMUV, Universitat de València, MALTA Consolider Team, Edificio de Investigación, c/ Dr. Moliner 50, 46100 Burjassot, Valencia, Spain*

[2]*DCITIMAC, MALTA Consolider Team, Facultad de Ciencias, Universidad de Cantabria, 39005 Santander, Spain*

[3]*Departamento de Física and Instituto de Materiales y Nanotecnología, MALTA Consolider Team, Universidad de La Laguna, 38206 La Laguna, Tenerife, Spain*

(Received 21 December 2021; revised 11 February 2022; accepted 10 March 2022; published 25 March 2022)

High-pressure optical-absorption measurements performed on polycrystalline $Co(IO_3)_2$ samples were used to characterize the influence of pressure on the electronic *d–d* transitions associated with $Co^{2+}$ and the fundamental band gap of $Co(IO_3)_2$. The results shed light on the electron-lattice coupling and show that $Co(IO_3)_2$ exhibits an unusual behavior because the compression of Co–O bond distances is not coupled to pressure-induced changes induced in the unit-cell volume. Experimental results on the internal *d–d* transitions of $Co^{2+}$ have been explained based on changes in the constituent $CoO_6$ octahedral units using the semiempirical Tanabe-Sugano diagram. Our findings support that the high-spin ground state ($^4T_1$) is very stable in $Co(IO_3)_2$. We have also determined the band-gap energy of $Co(IO_3)_2$ and its pressure dependence which is highly nonlinear. According to density-functional theory band-structure calculations, this nonlinearity occurs because the bottom of the conduction band is dominated by I-*5p* orbitals and the top of the valence band by Co-*3d* and O-*2p* orbitals, and because the Co–O and I–O bond lengths exhibit different pressure dependences.

DOI: 10.1103/PhysRevB.105.115204

## I. INTRODUCTION

The accurate characterization of the band-gap energy of semiconductors is fundamental for the development of electronic and optical applications. The study of the influence of pressure on the band-gap energy has gained interest over recent decades [1–3]. One of the reasons for the increasing interest is that high pressure (HP) has been shown to be an excellent tool to study the fundamental electronic properties of semiconductors [4,5]. In the case of cobalt iodate, $Co(IO_3)_2$, there is an interest in its band structure and band-gap energy. This is primarily motivated by its potential applications as a high-performance nonlinear-optical material [6]. The structural and vibrational properties of $Co(IO_3)_2$ have been characterized under HP [7], but as of yet there is no information on the band-gap energy or its pressure dependence. In addition to the optical absorptions associated with the fundamental band gap, there is an additional interest in $Co(IO_3)_2$. This interest is associated with the existence of internal intraconfigurational transitions within the $3d^7$ electron configuration of $Co^{2+}$ and with the 3*d* orbitals splitting caused by the octahedral crystal field [8]. These transitions are known as internal *d–d* transitions and are present in compounds with transition metals with partially occupied *d* shells (like $Mn^{2+}$, $Cu^{2+}$, and $Co^{2+}$). Such internal *d–d* transitions between localized states produce a weaker absorption (which is connected to the crystal field) compared to the fundamental absorption between the valence and conduction bands [9]. In particular, the pressure dependence of the *d–d* transitions is different from that of the fundamental band gap because they are governed by different physical mechanisms [10].

A compound like $Co(IO_3)_2$ can facilitate the experimental study of relevant electron-lattice couplings, like the Jahn-Teller (JT) effect, which involve orbital-degenerate electrons and lattice distortions or vibrations [9]. This electron-lattice coupling is responsible for a diverse range of phenomena, including colossal magnetoresistance, insulator-to-metal transitions, or spin transitions [11–14]. A deep understanding of electron-lattice coupling can be obtained from HP studies; therefore, the study of electron-lattice coupling under HP has become a key topic [3,5–7]. Octahedral $Co^{2+}$ oxides are particularly useful compounds for studying the influence of pressure on the electron-lattice coupling. In these compounds, the combined action of a weak JT effect ($T \otimes e$) and crystal anisotropy favors a low-symmetry distortion around the transition metal resulting in noncentrosymmetric octahedra. In addition, in octahedral $Co^{2+}$ oxides, *d–d* transitions result in weak optical-absorption bands with energies smaller than the band-gap energy. The energy of these bands is correlated to the crystal-field splitting of the $Co^{2+}$ $3d^7$ orbital in $CoO_6$ octahedral units, which is affected by the low-symmetry distortions. Therefore, optical-absorption (OA) spectroscopy under HP can provide important information to understand not only the HP behavior of the band gap, but also the pressure-induced changes in octahedral distortion, crystal-field strength, and spin configuration. Amongst the octahedral $Co^{2+}$ oxides, cobalt iodate, $Co(IO_3)_2$, is a particularly interesting compound which enables the experimental study of electron-lattice coupling under HP. This compound, with a monoclinic crystal structure at ambient conditions (space group $P2_1$) is extremely compressible (it

 

has a bulk modulus of 30 GPa) due to the lone electron pair of the $I^{5+}$ [7]. The crystal structure of $Co(IO_3)_2$ also shows a large anisotropic response to pressure [7]. Furthermore, the coordination polyhedra of $Co^{2+}$ and $I^{5+}$ are very sensitive to HP [8]. Due to these aspects of $Co(IO_3)_2$ outlined above, the application of low pressures ($< 20$ GPa) leads to important changes in the electron-lattice coupling and crystal field, making $Co(IO_3)_2$ an ideal prototype for studying correlations between electronic and crystal structures under compression.

Here, we report a combination of OA studies and density-functional theory (DFT) calculations on $Co(IO_3)_2$ under HP conditions. We show that changes in the fundamental band gap and internal $d$–$d$ absorption bands are intimately related to structural changes, thereby yielding an enhancement of the symmetry of $CoO_6$ octahedra under HP. The enhanced symmetry has a strong influence in the OA spectra due to the different electron-phonon couplings involved. The pressure evolution of the internal $d$–$d$ transitions and the fundamental band gap is explained by analyzing the crystal field and using DFT calculations.

## II. METHODS

### A. High-pressure optical-absorption experiments

HP optical-absorption experiments were carried out on a 3-$\mu$m-thin platelet of polycrystalline $Co(IO_3)_2$ which exhibited the $P2_1$ monoclinic structure [7]. The powder samples used in the present work were the same as those used for our previous study of the pressure-induced isostructural phase transition in $Co(IO_3)_2$. The crystal structure and sample purity of the $Co(IO_3)_2$ samples were reported in our previous work [7]. The optical-absorption measurements were performed in a diamond-anvil cell equipped with IIA-type diamonds with culet diameters of 480 $\mu$m. The sample was loaded in a 200-$\mu$m-diameter hole drilled in a stainless-steel gasket preindented to a thickness of 40 $\mu$m. Potassium bromide (KBr) was used as a pressure-transmitting medium (PTM) [15]. This medium is not fully hydrostatic above 2 GPa [15], but nonhydrostatic stresses do not substantially affect the behavior of $Co(IO_3)_2$ in the pressure range of our study, as shown in previous infrared studies [7]. In addition, KBr has the advantage of transparency in the energy range of optical-absorption experiments. The sample pressure was determined using the ruby scale [16]. The sample-in, sample-out method was used to acquire OA spectra using a bespoke optical setup [17]. The absorbance of the sample was obtained by normalizing the intensity of the light transmitted through the sample [$I(\omega)$] with the intensity of the light transmitted through the PTM [$I_0(\omega)$]. Further details regarding the optical-absorption setup can be found elsewhere [18]. Due to the difference in the intensity of the absorption of the band gap and internal $d$–$d$ transitions, the OA measurements were performed using two different light sources to separately investigate the visible and ultraviolet regions of the electromagnetic spectrum. The lower-energy region, 1.5 to 2.9 eV, allows an accurate measurement of the weak internal $d$–$d$ transitions of $Co^{2+}$. The higher-energy region, $>2.6$ eV, allows for measurement of the band-gap energy.

### B. First-principles calculations

The electronic properties of $Co(IO_3)_2$ were modeled within the framework of DFT [19] using the Vienna *Ab initio* Simulation Package (VASP). We used the generalized gradient approximation with the Armiento and Mattsson (AM05) prescription [20] for the exchange–correlation energy. Pseudopotentials were generated with the projector-augmented wave method [21] using a 540-eV plane-wave cutoff to ensure high accurate convergence. The Brillouin-zone $k$-point integration was carried out using a significant sampling of a $4 \times 6 \times 4$ grid for the primitive unit cell. The DFT + $U$ scheme [22] was used to treat the strongly correlated $3d$ states of Co atoms. In our calculations, we used an effective Hubbard parameter $U_{\text{eff}} = 3.32$ eV [7]. This parameter was optimized at ambient conditions and (as is common practice) assumed to be pressure independent [23,24]. This approach was shown to properly describe the changes induced by pressure in the crystal structure and phonons of $Co(IO_3)_2$ [7].

## III. RESULTS AND DISCUSSION

Figure 1 shows the absorbance spectra determined from a selection of OA spectra summarizing the pressure evolution of both the internal $d$–$d$ transitions [Fig. 1(a)] and the fundamental band gap [Fig. 1(b)]. In Fig. 1(a) we observe a change in the pressure evolution of absorptions associated with $d$–$d$ transitions at 7.3 GPa. In particular, the highest-energy band blueshifts with increasing pressure from ambient pressure to the highest pressure with a slope change at 7.3 GPa. This pressure of 7.3 GPa is close to the transition pressure of a previously reported isostructural phase transition [7]. This phase transition involves the enhancement of the symmetry of the $CoO_6$ octahedra and a change in the pressure dependence of Co–O bond distances. As we show, this fact is consistent with the observations of the present work. From the OA experiment data, we have obtained the pressure dependence of the $d$–$d$ transition energies by fitting Gaussian profiles to the absorption bands. The results are given in Fig. 2(c). In Fig. 1(b) it can be seen that the fundamental band gap redshifts as pressure increases. We later show that there are also changes in the pressure dependence of the band-gap energy near 7.3 GPa.

The data analysis indicates that changes in the optical properties are directly correlated to changes in the crystal structure, in particular, to local changes of the $CoO_6$ octahedra. In the crystal structure of $Co(IO_3)_2$ there are two Co atoms occupying nonequivalent crystallographic positions. However, their coordination octahedra are nearly identical [7]. A representation of the $CoO_6$ octahedra is provided in Fig. 2(a). From ambient pressure to 7.3 GPa the $CoO_6$ octahedra are noncentrosymmetric. At ambient conditions they have an average Co–O bond length of $r_0 = 2.067$ Å with a distortion index [$\sigma = (\sum_{i=1}^{6} (r_i - r_0)^2)^{1/2}$, and $r_0 = \frac{\sum_{i=1}^{6} r_i}{6}$] of $\sigma = 0.06$ Å according to DFT calculations [25]. The pressure dependence of $\sigma$ is represented in Fig. 2(d). The oxygen-metal (Co and Zn) bond distances used to calculate the distortion index were obtained from previously reported DFT calculations [7,26]. The distortion index of the $CoO_6$ octahedra initially decreases very rapidly with pressure. At 7.3 GPa, $r_0 = 2.046$ Å and $\sigma = 0.02$ Å. After the phase transition at 7.3 GPa, the

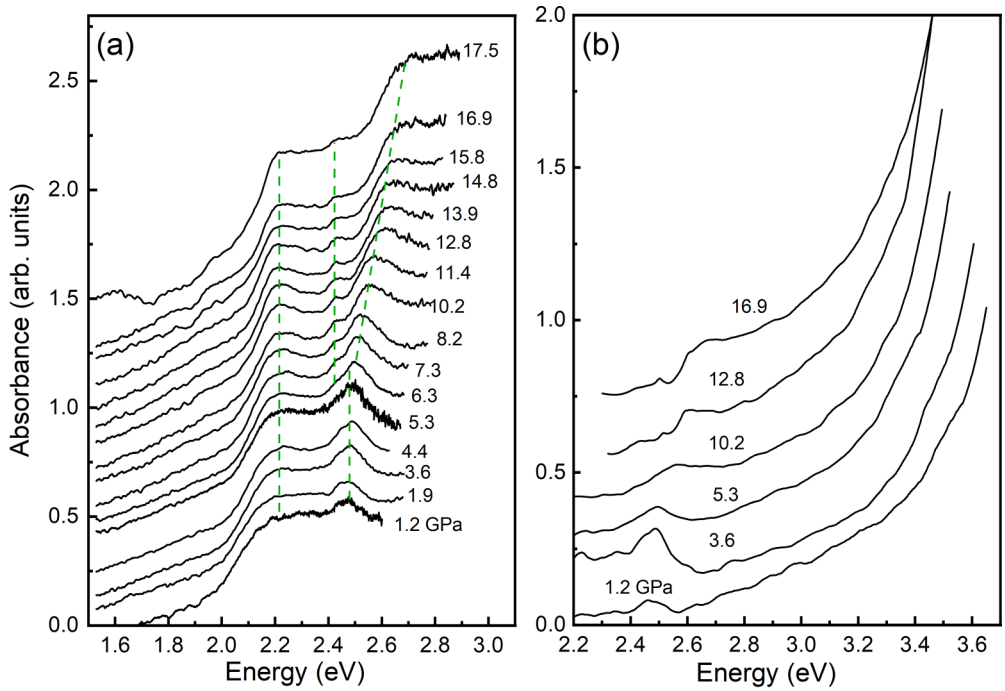


FIG. 1. High-pressure optical-absorption spectra of $Co(IO_3)_2$. (a) The lower-energy region, 1.5 to 3.1 eV, selected to highlight the weak internal $d$–$d$ absorption bands. (b) The higher-energy region, 2.2 to 3.7 eV, selected to show the fundmanetal band-gap absorption. Pressures in GPa are indicated in the figures. Different light sources were used in (a) and (b) corresponding to the different energy regions. In (a), the green lines show the pressure evolution of $Co^{2+}$ $d$–$d$ bands. The absorbance was obtained by the function $A = \log_{10} \frac{I(\omega)}{I_0(\omega)}$, where $A$ is absorbance, and $I(\omega)$ and $I_0(\omega)$ are, respectively, the light transmitted through the sample and the PTM.

rate of change of distortion index with increasing pressure is much lower, despite the fact that the Co–O bond lengths continue to decrease, eventually reaching values of $r_0 = 2.029$ Å and $\sigma = 0.01$ Å at 17.5 GPa. Therefore, the $CoO_6$ octahedra become more symmetric with increasing pressure, eventually becoming quasicentrosymmetric beyond 7.3 GPa. As shown in Fig. 2(d), the two inequivalent $CoO_6$ octahedra exhibit the same pressure dependence of the distortion index $\sigma$. This means that, to a first approximation, we can analyze the OA spectra with a model including only one effective $CoO_6$ octahedron.

The octahedral distortion in $Co(IO_3)_2$ probably arises from structural modifications induced by the crystal anisotropy and the weak Jahn-Teller effect ($T \otimes e$) associated with the $t_{2g}$ orbitals [the $^4T_{1g}(F)$ ground state] [27–29]. Thus, the octahedral distortion affects the crystal-field splitting of the $Co^{2+}$ ($3d^7$) orbitals in $CoO_6$ under HP as we show in the one-electron energy-level diagram given in Fig. 2(b). The splitting of the parent octahedral $t_{2g}(\Delta_t)$ and $e_g(\Delta_e)$ orbitals was estimated through correlations between the low-symmetry local structure and both $\Delta_e$ and $\Delta_t$ established elsewhere for halides and oxides [9,27–29]. For an octahedral distortion of $\sigma = 0.06$ Å, we estimate $\Delta_e$ of about 0.2–0.3 eV and $\Delta_t$ of about 0.05 eV at ambient conditions, both of which decrease by a factor of 6 by 17.5 GPa. As discussed later in the present work, the reduction of the crystal-field splitting with increasing pressure yields a narrowing of the $d$–$d$ absorption band at 2.15 eV [see Fig. 1(a)]. The $Co^{2+}$ cation in $Co(IO_3)_2$ has a $3d^7$ electronic configuration wherein the seven $3d$ electrons occupy the $d_{xy}$, $d_{xz}$, $d_{yz}$, $d_{x^2-y^2}$, and $d_{z^2}$ orbitals with five electrons in triply degenerate $t_{2g}$ level and two spin-up electrons in the doubly degenerate $e_g$ level, both of which are split by $\Delta_t$ and $\Delta_e$, respectively, in the $O_h$-distorted $CoO_6$ octahedron.

In sixfold-coordinated $Co^{2+}$, in nearly octahedral coordination, the absorption bands originating from $d$–$d$ transitions can be well described using the Tanabe-Sugano (TS) diagram for octahedral $Co^{2+}$ ($3d^7$) [30]. This diagram is shown in Fig. 3. The TS diagram is based on a semiempirical model that describes the internal $d$–$d$ transitions using the crystal-field splitting energy, $\Delta$, and the interelectronic repulsion interactions through the Racah parameters $B$ and $C$ [31]. The energies of all possible transitions from the ground state can be precisely described through these three parameters and they are represented through the Tanabe-Sugano diagram [32]. In the high-spin state of $Co^{2+}$, the only spin-allowed transitions are: $^4T_{1g}(F) \rightarrow {}^4T_{2g}(F)$, $^4T_{1g}(F) \rightarrow {}^4A_{2g}(F)$, $^4T_{1g}(F) \rightarrow {}^4T_{1g}(P)$. Amongst them, the $^4T_{1g}(F) \rightarrow {}^4T_{1g}(P)$ transition shows the maximum oscillator strength and a relatively narrow full width at half maximum (FWHM). The $^4T_{1g}(F) \rightarrow {}^4T_{2g}(F)$ transition energy, which is proportional to the crystal-field splitting $\Delta$, is below the explored spectral range (at about 0.7 eV). Furthermore, the energy of the $^4T_{1g}(F) \rightarrow {}^4A_{2g}(F)$ transition, involving two electrons jumping from $t_{2g}$ to $e_g$, is proportional to $2\Delta$, giving rise to strong electron-phonon couplings, yielding a band broadening and thus being difficult to detect at ambient conditions. Examples of this behavior can be found in $KCoF_3$, $CoF_2$ [33], and $CoCl_2$ [34]. Therefore, the $^4T_{1g}(F) \rightarrow {}^4T_{1g}(P)$ transition is the major feature of the OA spectra of these compounds, and it is responsible for their characteristic red color. Therefore, the band placed at 2.13 eV at 1.2 GPa in $Co(IO_3)_2$ [see Fig. 1(a)] can be assigned to the spin-allowed $^4T_{1g}(F) \rightarrow {}^4T_{1g}(P)$ transition. Additionally,

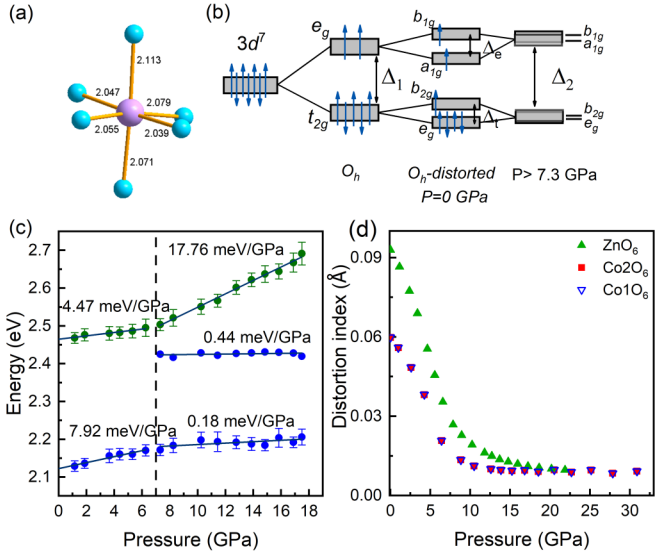


FIG. 2. (a) Representation of the $CoO_6$ octahedron. (b) Diagram of $Co^{2+}$ $d$ levels in $Co(IO_3)_2$ for $P < 7.3$ GPa and $P > 7.3$ GPa. (c) Pressure dependence of the $d$–$d$ transition energies. The solid lines are linear fits. The vertical dashed line indicates the phase transition pressure. Where not visible the error bars are smaller than symbols. (d) Distortion index of $Co1O_6$ and $Co2O_6$ in $Co(IO_3)_2$ compared to that of $ZnO_6$ in $Zn(IO_3)_2$. The bond distance between the metal (Co and Zn) and iodine used to calculate the distortion index was obtained from DFT calculations [7].

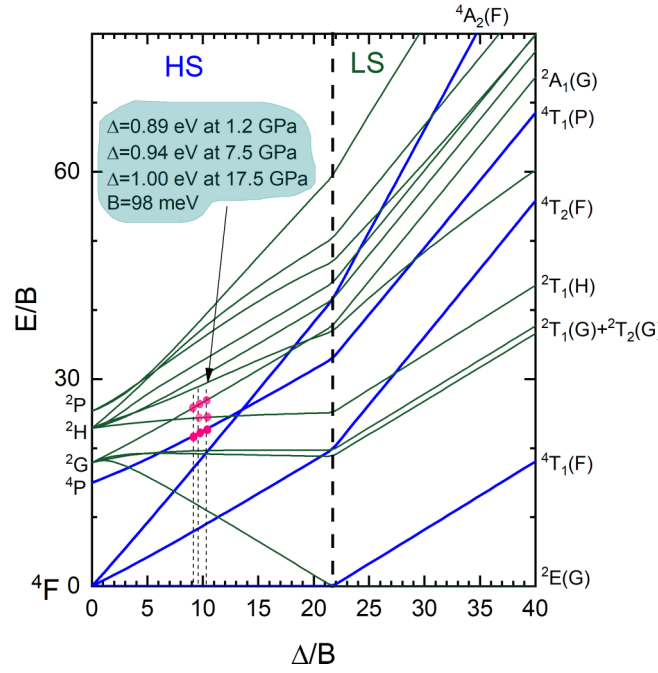


FIG. 3. TS diagram for $3d^7$ ions calculated for $C/B = 4.62$. The state energy is a function of the crystal-field energy $\Delta$ in terms of the Racah parameter $B$. For clarity, only relevant energy states are plotted. Blue (green) lines represent states where the transtion is spin allowed (forbidden). Red dots correspond to selected spectroscopic data at different pressures. The vertical dashed line shows the high-spin (HS, $S = 3/2$) to low-spin (LS, $S = 1/2$) crossover at $\Delta/B = 22$.

the weaker absorption band at 2.47 eV is associated with the ${}^4T_{1g}(F) \rightarrow {}^2A_{1g}(G)$ transition. Although this transition is initially spin forbidden by the electric dipole (ED) mechanism, the spin-orbit interaction and the proximity of charge-transfer states make it ED allowed. The pressure coefficients of these bands [Fig. 2(c)] support the present assignment. Other bands are difficult to identify in the absorption spectra due to their broad FWHM, especially at lower pressures ($P < 7.3$ GPa).

An important feature in the pressure evolution of the absorption spectra is the progressive band narrowing experienced by the absorption bands above 7.3 GPa. This narrowing allows us to clearly resolve the narrow spin-fliplike ${}^4T_{1g}(F) \rightarrow {}^2T_{1g}(H)$ transition at 2.43 eV, and the oscillator-strength enhanced ${}^4T_{1g}(F) \rightarrow {}^2A_{1g}(G)$ transition that blueshifts with pressure from 2.52 to 2.63 eV when increasing pressure from 7.5 to 17.5 GPa, This pressure-induced narrowing of all $d$–$d$ absorption bands correlates with the symmetrization of the $CoO_6$ octahedra with pressure, as indicated by the progressive decrease of the octahedral distortion index, $\sigma$, from 0.06 at ambient pressure, to 0.01 Å at 17.5 GPa; see Fig. 2(d). The homogeneous band narrowing is associated with the reduction of the FWHM due to the $e_g$ splitting $\Delta_e$. The energy-level splitting is represented in Fig. 2(b). The band energies and their variation with pressure can be described based on the TS diagram given in Fig. 3. According to the transition assignment in the TS diagram, the energy ratio between the two $d$–$d$ transition bands observed in experiments at 1.2 GPa is 2.47 eV/2.13 eV = 1.16. The same ratio between states ${}^2A_{1g}(G)$ and ${}^4T_{1g}(P)$ in the TS diagram corresponds to $\Delta/B = 9.08$ ($x$ axis) and $E/B = 21.7$ ($y$ axis), when $E = 2.13$ eV. Thus, the Racah parameters $B = 0.098$ eV, $C = 0.453$ eV, and the crystal-field splitting $\Delta = 0.89$ eV at 1.2 GPa are consistent with the nephelauxetic series [35]. In particular, $B$ is similar to the parameters obtained at ambient pressure in $KCoF_3$ ($Co^{2+}$), $B = 0.105$ eV ($\Delta = 0.95$ eV) [33], in $CoCl_2$ ($Co^{2+}$), $B = 0.097$ eV ($\Delta = 0.87$ eV) [34], in CoO ($Co^{2+}$), $B = 0.105$ eV ($\Delta = 1.15$ eV) [35], and in the hexa-aquo $Co(OH_2)_6$ complex, which has $Co^{2+}$ octahedrally surrounded oxygen atoms, $B = 0.073$ eV ($\Delta = 1.12$ eV) [35], and it is higher than that found in $MnWO_4$ ($Mn^{2+}O_6$), $B = 0.077$ eV ($\Delta = 0.94$ eV) [36], which is reasonable as $Mn^{2+}$ has a $d^5$ configuration.

It is worth noting that the pressure-induced band narrowing of the $d$–$d$ bands observed in the optical spectra above 7.3 GPa is a sign of the suppression of the low-symmetry distortion of the $CoO_6$ octahedra due, in part, to the Jahn-Teller effect associated with the ${}^4T_{1g}(F)$ ground state. The symmetry enhancement of the divalent metal coordination octahedra is not a feature unique to HP $Co(IO_3)_2$. It also happens in other metal iodates such as $Fe(IO_3)_3$ [37] and $Zn(IO_3)_2$ [26], as can be seen in Fig. 2(d), where the distortion index of $ZnO_6$ is compared with that of $CoO_6$. However, the $d$–$d$ absorption bands of other metal iodates are typically not observable in their OA spectra. Therefore, $Co(IO_3)_2$ provides a unique way to investigate the pressure evolution of metal oxygen complexes in metal iodates.

From the data shown in Fig. 2(c) it can be deduced that the crystal-field splitting in the $CoO_6$ octahedra is enhanced under pressure. This phenomenon is a direct consequence of the volume reduction upon compression of the crystal structure of

$Co(IO_3)_2$ which yields a reduction in the Co–O bond distance. We have found a variation of $\Delta$ from 0.89 at 1.2 GPa, to 1.00 eV at 17.5 GPa; see Fig. 3. Interestingly, this fact is consistent with expectations of the crystal- (or ligand-) field theory (CFT). According to CFT, $\Delta/\Delta_0 = (r_0/r)^n$ with the $n$ exponent close to 5 [29]. This relationship is usually employed with $(V_0/V)^{n/3}$ since the volumes can be more easily obtained by, for example, the equation of state determined by x-ray diffraction [7]. The corresponding bond distances $r(P)$, on the other hand, often require single-crystal x-ray diffraction (XRD) measurements. The approach utilizing $(V_0/V)^{n/3}$ is correct provided that the bond distances scale proportionally to the crystal volume with pressure [29]. The results obtained from $Co(IO_3)_2$ in the present work provide a primary example of how the Co–O bond distances and unit-cells volumes can scale disproportionately; therefore, in the present case of $Co(IO_3)_2$, the approximation $\Delta/\Delta_0 = (V_0/V)^{n/3}$ is no longer valid. Considering the variations of $\Delta$, $V$, and $r$ we obtain exponents of $n = 3(1)$ and 6(1) using $(V_0/V)^{n/3}$ and $(r_0/r)^n$, respectively, the latter being compatible with crystal-field theory expectations of $n = 5$. The large difference between the exponents acquired using different assumption reveals that the reduction in the average volume per atom in the crystal structure upon compression is mainly accounted for by the iodine coordination polyhedra (which are more compressible due to the presence of a lone electron pair on the $I^{5+}$ cation,) rather than the $CoO_6$ octahedra. This also reveals that the I–O bonds are more compressible than the Co–O bonds.

Another interesting feature to explore from our results is the possible occurrence of a spin transition in $Co(IO_3)_2$. Using the TS diagram, the critical pressure for the high-spin to low-spin crossover can be estimated. According to Fig. 3, this is expected to happen at $\Delta/B = 22$ ($\Delta = 2.2$ eV). Based on these results, the corresponding volume reduction needed to reach $\Delta = 2.2$ eV would be about 60%, which would be equivalent to a pressure of about 110 GPa, according to results from XRD studies [7]. This pressure is much higher than the spin-crossover transition pressure found in $CoCl_2$ (near 70 GPa) [34]. This result indicates that the high-spin state is very stable in $Co(IO_3)_2$.

To conclude, we discuss the pressure dependence of the band gap. According to our band-structure calculations, $Co(IO_3)_2$ has an indirect band gap, as is observed in other metal iodates [38]. Based on the assumption of an indirect band gap, we have determined the pressure dependence of the band-gap energy from the OA spectra measured in the high-energy range. The values of the indirect band-gap energy were determined using a Tauc plot analysis [39], wherein the linear fit of the high-energy part of the $(\alpha h\upsilon)^{1/2}$ vs $h\upsilon$ plot was extrapolated to $(\alpha h\upsilon)^{1/2} = 0$, where $\alpha$ is the absorption coefficient, $h$ is Plank's constant, and $\upsilon$ is the photon's frequency. The value of the band-gap energy was thereby estimated to be 3.5(1) eV at 1.2 GPa, which is similar to that of the structurally related metal iodate $Zn(IO_3)_2$ [40]. The pressure dependence of the band-gap energy is shown in Fig. 4, where the experimental results are compared with those derived from our DFT calculations. The DFT calculations underestimate the band-gap energy at ambient pressure, giving a value of 2.26 eV; however, they provide a good description of the pressure dependence of the band-gap energy. The difference between

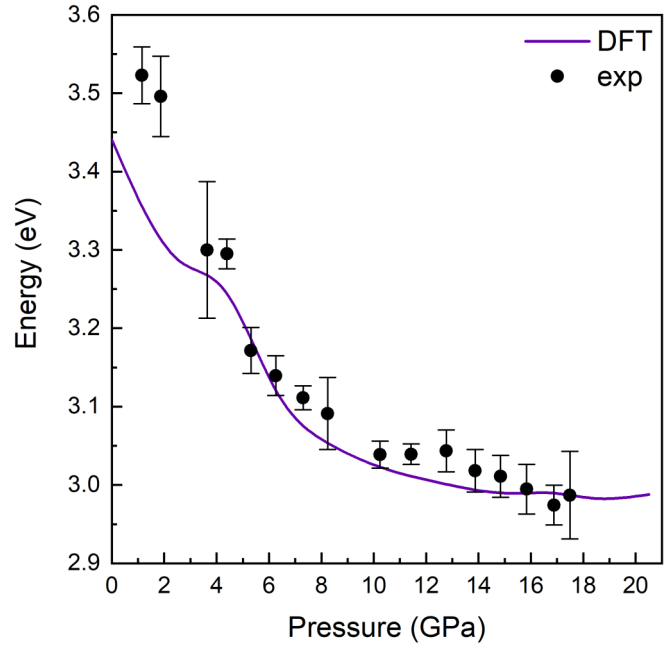


FIG. 4. Pressure dependence of the band gap of $Co(IO_3)_2$. Data from experiments and DFT calculations are, respectively, shown with symbols and with a solid line. The calculated band gap has been offset by 1.2 eV to facilitate comparison as discussed in the main text.

measured and calculated band gaps at ambient pressure is typical of DFT calculations and it is related to the approximations used to describe the exchange and correlation energies. However, the underestimation of the absolute value of the band gap does not affect the calculated relative changes induced by pressure [41,42], as is shown by the good agreement between experiment and theory in Fig. 4, where the calculated band gap has been offset by 1.2 eV to facilitate comparison. In the figure it can be seen that the band-gap energy decreases rapidly from 3.5 eV at ambient pressure to 3.1 eV at 8 GPa. Above 8 GPa, the band-gap energy decreases much more slowly, eventually reaching a value of 3 eV at 18 GPa.

In Fig. 5 we present the electronic density of states (DOS) and projected density of states (PDOS) at ambient pressure. The pressure dependence of the atomic character in the valence-band maximum (VBM) and conduction-band minimum (CBM) are shown in Fig. 6, where we can observe that the VBM is dominated by the Co-3$d$ and O-2$p$ orbitals, and the CBM is dominated by the I-5$p$ orbitals, with some contribution from the O-2$p$ orbitals. Thus, the band-gap energy will be strongly affected by changes in the Co–O and I–O bond distances. As we have reported previously [7], the Co–O bond distances decrease from ambient pressure (2.067 Å) to around 7 GPa (2.046 Å), after which pressure the distance continues to decease but more slowly. On the other hand, the length of the I–O bonds in the original $IO_3$ polyhedron (a trigonal pyramid) continuously increases under compression, in order to accommodate the three second-nearest neighboring oxygen atoms, thereby gradually transforming the original $IO_3$ polyhedron into an $IO_6$ distorted octahedron. Consequently, there are two competing effects affecting the states near the Fermi level under compression. The decrease of the Co–O bond

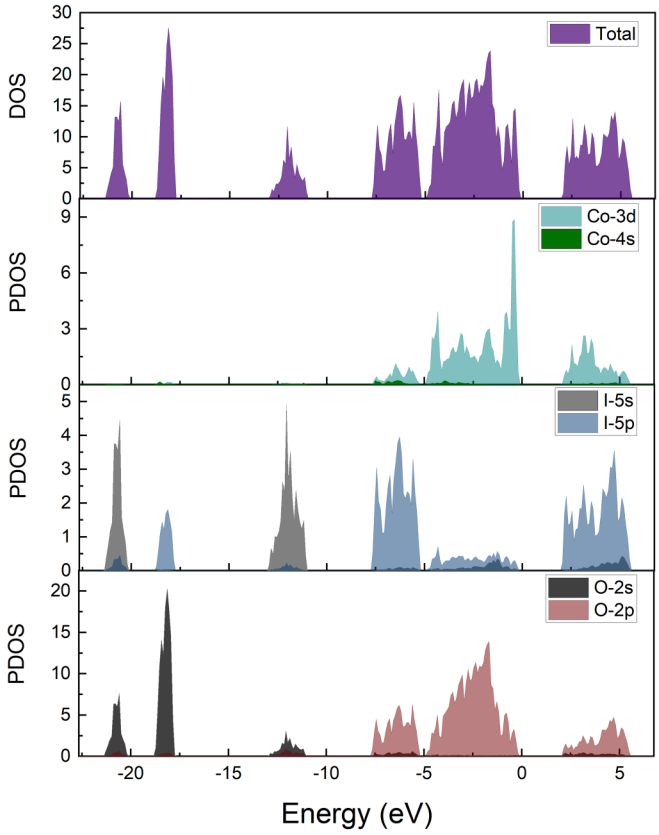


FIG. 5. Calculated total electronic DOS and PDOS for $Co(IO_3)_2$ at ambient pressure.

distances enhances the overlap between Co and O orbitals, favoring the narrowing of the band-gap energy. In contrast, the increase of the three I–O bond distances reduces the hybridization between iodine and oxygen, which favors the opening of the band gap. At lower pressures, the large contribution of Co states to the VBM dominates the change of the band-gap energy, so the band gap decreases with pressure, up to around 8 GPa. Beyond this pressure, the two effects neutralize each other, and the band gap of $Co(IO_3)_2$ almost remains unchanged under increasing pressure. A consequence of the competition between the two mechanisms described above is a small shoulder in the pressure dependence of the band gap predicted by calculations around 4 GPa. This shoulder is not observed in experiments, probably due to the associated experimental error.

## IV. CONCLUSIONS

In conclusion, optical-absorption measurements of $Co(IO_3)_2$ provide useful information regarding the electron-lattice coupling of this $Co^{2+}$ compound. In particular, we have been able to determine that the pressure evolution of

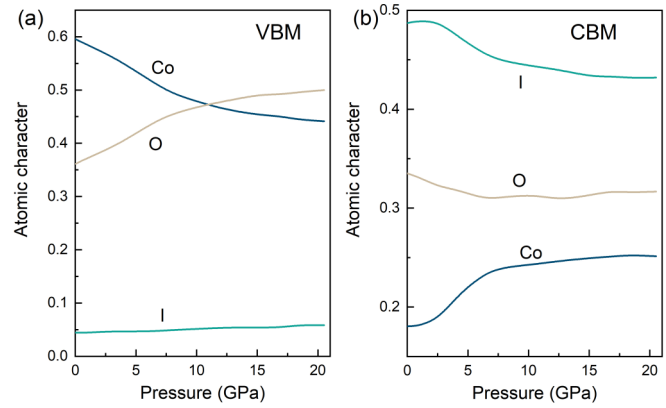


FIG. 6. Calculated pressure dependence of the normalized atomic character in (a) the VBM and (b) CBM of the electronic band structure in $Co(IO_3)_2$.

the $d$–$d$ transitions in $Co(IO_3)_2$ is distinct from that observed in other $Co^{2+}$ compounds, and that, therefore, $Co(IO_3)_2$ provides a primary example of how the pressure dependencies of volume and Co–O bond distances can be decoupled. We have correlated the large broadening of $d$–$d$ bands at ambient conditions with the low-symmetry octahedral distortion of $CoO_6$ that additionally splits the $e_g$ and $t_{2g}$ $Co^{2+}$ orbitals. The pressure-induced band narrowing is thus associated with the symmetrization of the $CoO_6$ octahedra, that in turn unveils the existence of a structural phase transition at 7.3 GPa. Additionally, we have found that changes in the $d$–$d$ transition energies also support the existence of such a phase transition. Using the Tanabe-Sugano diagram we have provided a rational explanation for all observed results. Based on this analysis, we concluded that the high-spin state is very stable in $Co(IO_3)_2$, and the high-spin to low-spin transition could be expected in the 110-GPa range. Finally, it was determined that the band-gap energy follows a strong nonlinear pressure dependence, with a change in slope near the transition pressure. An explanation for this behavior is provided based upon DFT band-structure calculations.

## ACKNOWLEDGMENTS

This work was supported by the Generalitat Valenciana under Project No. PROMETEO 2018/123-EFIMAT and by the Spanish Research Agency (AEI) and Spanish Ministry of Science and Investigation (MCIN) under Projects No. PID2019106383GB-C41/C43 (DOI: 10.13039/501100011033) cofinanced by EU FEDER funds, No. PGC2018-101464-B-I00, and No. RED2018-102612-T. A.L. and D.E. thank the Generalitat Valenciana for the Ph.D. Fellowship No. GRISOLIAP/2019/025. R.T. acknowledges funding from the Spanish MINECO via the Juan de la Cierva Formación program (Grant No. FJC2018-036185-I).

[1] J. Ibáñez, A. Segura, B. García-Domene, R. Oliva, F. J. Manjón, T. Yamaguchi, Y. Nanishi, and L. Artús, Phys. Rev. B **86**, 035210 (2012).

[2] R. Lacomba-Perales, D. Errandonea, A. Segura, J. Ruiz-Fuertes, P. Rodríguez-Hernández, S. Radescu, J. López-Solano, A. Mujica, and A. Muñoz, J. Appl. Phys. **110**, 043703 (2011).

[3] E. Bandiello, J. Sánchez-Martín, D. Errandonea, and M. Bettinelli, Crystals **9**, 237 (2019).

[4] P. Botella, D. Errandonea, A. B. Garg, P. Rodriguez-Hernandez, A. Muñoz, S. N. Achary, and A. Vomiero, SN Appl. Sci. **1**, 389 (2019).

[5] F. J. Manjón, D. Errandonea, A. Segura, A. Muñoz, G. Tobías, P. Ordejón, and E. Canadell, Phys. Rev. B **63**, 125330 (2001).

[6] C. L. Hu and J. G. Mao, Coord. Chem. Rev. **288**, 1 (2015).

[7] A. Liang, C. Popescu, F. J. Manjon, R. Turnbull, E. Bandiello, P. Rodriguez-Hernandez, A. Muñoz, I. Yousef, Z. Hebboul, and D. Errandonea, J. Phys. Chem. C **125**, 17448 (2021).

[8] F. Rodríguez, D. Hernández, J. Garcia-Jaca, H. Ehrenberg, and H. Weitzel, Phys. Rev. B **61**, 16497 (2000).

[9] J. Ruiz-Fuertes, A. Segura, F. Rodríguez, D. Errandonea, and M. N. Sanz-Ortiz, Phys. Rev. Lett. **108**, 166402 (2012).

[10] E. Jara, J. A. Barreda-Argüeso, J. González, R. Valiente, and F. Rodríguez, Pap. Phys. **11**, 110004 (2019).

[11] M. R. Otto, J. H. Pöhls, L. P. René de Cotret, M. J. Stern, M. Sutton, and B. J. Siwick, Sci. Adv. **7**, edbf2810 (2021).

[12] I. Loa, P. Adler, A. Grzechnik, K. Syassen, U. Schwarz, M. Hanfland, G. Kh. Rozenberg, P. Gorodetsky, and M. P. Pasternak, Phys. Rev. Lett. **87**, 125501 (2001).

[13] M. Baldini, V. V. Struzhkin, A. F. Goncharov, P. Postorino, and W. L. Mao, Phys. Rev. Lett. **106**, 066402 (2011).

[14] K. Liu, C. Li, T. Wen, D. Jiang, Z. Jiang, Y. Ma, and Y. Wang, Chem. Asian J. **16**, 3437 (2021).

[15] J. Zhao and N. L. Ross, J. Phys.: Condens. Matter **27**, 185402 (2015).

[16] H. K. Mao, J. Xu, and P. M. Bell, J. Geophys. Res. **91**, 4673 (1986).

[17] A. Segura, J. A. Sans, D. Errandonea, D. Martinez-García, and V. Fages, Appl. Phys. Lett. **88**, 011910 (2006).

[18] D. Errandonea, C. Popescu, A. B. Garg, P. Botella, D. Martinez-García, J. Pellicer-Porres, P. Rodríguez-Hernández, A. Muñoz, V. Cuenca-Gotor, and J. A. Sans, Phys. Rev. B **93**, 035204 (2016).

[19] P. Hohenberg and W. Kohn, Phys. Rev. **136**, B864 (1964).

[20] A. E. Mattsson and R. Armiento, Phys. Rev. B **79**, 155101 (2009).

[21] P. E. Blöchl, Phys. Rev. B **50**, 17953 (1994).

[22] S. L. Dudarev, G. A. Botton, S. Y. Savrasov, C. J. Humphreys, and A. P. Sutton, Phys. Rev. B **57**, 1505 (1998).

[23] O. Bengone, M. Alouani, P. Blöchl, and J. Hugel, Phys. Rev. B **62**, 16392 (2000).

[24] S. A. Tolba, K. M. Gameel, B. A. Ali, H. A. Almossalami, and N. K. Allam, in *Density Functional Calculations: Recent Progresses of Theory and Application*, The DFT+U: Approaches, Accuracy, and Applications, edited by G. Yang (IntechOpen, London, 2018), pp. 3–30.

[25] A. Y. Ramos, H. C. N. Tolentino, N. M. Souza-Neto, J. P. Itié, L. Morales, and A. Caneiro, Phys. Rev. B **75**, 052103 (2007).

[26] A. Liang, C. Popescu, F. J. Manjon, P. Rodriguez-Hernandez, A. Muñoz, Z. Hebboul, and D. Errandonea, Phys. Rev. B **103**, 054102 (2021).

[27] F. Aguado, F. Rodríguez, and P. Núñez, Phys. Rev. B **67**, 205101 (2003).

[28] F. Aguado, F. Rodríguez, and P. Núñez, Phys. Rev. B **76**, 094417 (2007).

[29] M. N. Sanz-Ortiz and F. Rodríguez, J. Chem. Phys. **131**, 124512 (2009).

[30] Y. Tanabe and S. Sugano, J. Phys. Soc. Jpn. **9**, 753 (1954).

[31] M. Atanasov, D. Ganyushin, K. Sivalingam, and F. Neese, in *Molecular Electronic Structures of Transition Metal Complexes II*, A Modern First-Principles View on Ligand Field Theory through the Eyes of Correlated Multireference Wavefunctions, edited by D. M. P. Mingos, P. Day, and J. P. Dahl (Springer Science & Business Media, Berlin, 2012), pp. 149–220.

[32] L. Nataf, F. Rodríguez, and R. Valiente, Phys. Rev. B **86**, 125123 (2012).

[33] J. A. Barreda-Argüeso, F. Aguado, J. González, R. Valiente, L. Nataf, M. N. Sanz-Ortiz, and F. Rodríguez, J. Phys. Chem. C **120**, 18788 (2016).

[34] J. A. Barreda-Argüeso, L. Nataf, F. Aguado, I. Hernández, J. González, A. Otero-de-la-Roza, V. Luaña, Y. Jia, C. Jin, B. Kim, K. Kim, B. I. Min, W. Heribert, A. P. Jephcoat, and F. Rodríguez, Sci. Rep. **9**, 5448 (2019).

[35] R. G. Burns, *Mineralogical Applications of Crystal Field Theory* (Cambridge University Press, Cambridge, 1993).

[36] J. Ruiz-Fuertes, S. López-Moreno, J. López-Solano, D. Errandonea, A. Segura, R. Lacomba-Perales, A. Muñoz, S. Radescu, P. Rodríguez-Hernández, M. Gospodinov, L. L. Nagornaya, and C. Y. Tu, Phys. Rev. B **86**, 125202 (2012).

[37] A. Liang, S. Rahman, H. Saqib, P. Rodriguez-Hernandez, A. Munoz, G. Nenert, I. Yousef, C. Popescu, and D. Errandonea, J. Phys. Chem. C **124**, 8669 (2020).

[38] A. Liang, P. Rodríguez-Hernandez, A. Munoz, S. Raman, A. Segura, and D. Errandonea, Inorg. Chem. Front. **8**, 4780 (2021).

[39] J. Tauc, Mater. Res. Bull. **3**, 37 (1968).

[40] A. Benghia, Z. Hebboul, R. Chikhaoui, I. Khaldoun Lefkaier, A. Chouireb, and S. Goumri-Said, Vacuum **181**, 109660 (2020).

[41] A. Liang, L. T. Shi, S. Gallego-Parra, O. Gomis, D. Errandonea, and I. M. Tiginyanu, J. Alloys Compd. **886**, 161226 (2021).

[42] A. Mujica, A. Rubio, A. Muñoz, and R. J. Needs, Rev. Mod. Phys. **75**, 863 (2003).